AIP Journal of Applied Physics

Raman tensor elements and Faust-Henry coefficients of wurtzite-type α-GaN: How to overcome the dilemma of the sign of Faust-Henry coefficients in α-GaN?

Gert Irmer, Christian Röder, Cameliu Himcinschi, and Jens Kortus

Citation: Journal of Applied Physics **116**, 245702 (2014); doi: 10.1063/1.4904841
View online: http://dx.doi.org/10.1063/1.4904841
View Table of Contents: http://scitation.aip.org/content/aip/journal/jap/116/24?ver=pdfcov
Published by the AIP Publishing

Raman tensor elements and Faust-Henry coefficients of wurtzite-type α-GaN: How to overcome the dilemma of the sign of Faust-Henry coefficients in α-GaN?

Gert Irmer,[a] Christian Röder, Cameliu Himcinschi, and Jens Kortus
TU Bergakademie Freiberg, Institute of Theoretical Physics, Leipziger Str. 23, D-09599 Freiberg, Germany

(Received 7 October 2014; accepted 26 November 2014; published online 29 December 2014)

Faust-Henry coefficients are ratios describing the relative influence of lattice displacements and electric field onto the electric susceptibility. They are essential in order to access the charge carrier concentration as well as the mobility of polar semiconductors by Raman scattering from measured frequencies, bandwidths, and intensities of coupled phonon-plasmon modes. In the case of α-GaN only the Faust-Henry coefficient connected with the Raman tensor elements a_{TO} and a_{LO} of the axial modes has been reported with differing results and questionable sign. However, according to its wurtzite structure, in hexagonal GaN three Faust-Henry coefficients associated with phonon modes of different symmetry exist. In the present study, from Raman scattering efficiencies of corresponding transverse optical and longitudinal optical phonons which are accessible in different scattering configurations, Raman tensor elements, and respective Faust-Henry coefficients were deduced. It is shown that near-forward scattering of phonon-polaritons, depending on frequency, allows the unambiguous determination of the sign of Faust-Henry coefficients. In case of α-GaN the obtained Faust-Henry coefficients connected with the corresponding Raman tensor elements are $C_a^{FH} = -3.46$, $C_b^{FH} = -3.81$, and $C_c^{FH} = -2.31$. © *2014 AIP Publishing LLC*.
[http://dx.doi.org/10.1063/1.4904841]

I. INTRODUCTION

GaN and its ternary alloys with Al and In are a remarkable and the most important materials system for several electronic and short-wavelength optoelectronic applications. GaN based microelectronic devices, for example, take advantage of the superior electronic properties for high power, high frequency, and high temperature applications. Furthermore, the group III nitride semiconductors with direct bandgaps ranging from 0.7 eV (InN) through 3.4 eV (GaN) to 6.0 eV (AlN) have inspired the field of solid-state lighting. In particular, applications of these materials realizing bright, white LEDs appear very promising.[1–5]

Depending on the application of GaN, numerous Raman scattering studies have been performed characterizing its properties, i.e., residual stress analysis[6,7] or the determination of charge carrier concentration and mobility.[8–11] In order to access the charge carrier concentration as well as the mobility by Raman scattering from measured frequencies, bandwidths, and intensities of coupled phonon-plasmon modes,[12–14] knowledge of the Faust-Henry coefficients is required. These coefficients are ratios describing the relative influence of lattice displacements and electric field onto the electric susceptibility.[12,15,16] In the case of α-GaN merely the Faust-Henry coefficient connected with the polar phonon mode of A_1 symmetry and its assigned Raman tensor elements a_{TO} and a_{LO} has been reported with differing values and questionable sign in literature.[17–21] However, according to its wurtzite structure, in hexagonal GaN three Faust-Henry coefficients associated with phonon modes of different symmetry exist. Besides the general interest in this material, our investigation of GaN was also stimulated by the fact that nowadays large and pure single crystals are available. In this work, Raman measurements on undoped α-GaN single crystals were performed using different scattering geometries, i.e., 180°, 90°, and 0°, in order to access Raman scattering efficiencies of corresponding transverse optical (TO) and longitudinal optical (LO) phonons. From the obtained Raman scattering efficiencies, the absolute value of each Raman tensor element as well as the respective Faust-Henry coefficients were deduced. Furthermore, it is shown that near-forward scattering of phonon-polaritons, depending on frequency, allows one to overcome the dilemma of the sign of Faust-Henry coefficients unambiguously. Depending on the sign of the Faust-Henry coefficients contributions of the lattice displacements and the electric field associated with them to the Raman scattering efficiency interfere constructively or destructively.

This paper is organized as follows: First, a detailed derivation of the theoretical Raman scattering efficiency of the three polar phonon modes in wurtzite-type crystals is given. Second, we report on systematic Raman measurements in order to determine the Raman scattering efficiencies of the A_1(TO), A_1(LO), E_1(TO), and E_1(LO) phonons which requires the application of different scattering geometries. The Faust-Henry coefficients are calculated based on the ratio of the measured Raman efficiency of the TO-phonon to the one of the LO-phonon. However, in each case two solutions are obtained. The measurement of phonon-polariton Raman efficiencies then enables one to assign one solution unambiguously.

[a]Author to whom correspondence should be addressed. Electronic mail: irmer@physik.tu-freiberg.de

II. THEORY

A. Phonon modes in α-GaN

The primitive unit cell of α-GaN with space group C_{6v}^4 contains four atoms. One Ga atom of the two GaN pairs is tetrahedrally coordinated by four N atoms, and vice versa. Group theory predicts $3 \times 4 = 12$ phonon normal modes at the Γ-point of the Brillouin zone according to the irreducible representation $2A_1 + 2B_1 + 2E_1 + 2E_2$. One set of A_1 and E_1 modes are acoustic, while the remaining $A_1 + 2B_1 + E_1 + 2E_2$ modes are optical ones. The A_1 and E_1 modes are both Raman and IR (infrared) active, the two E_2 modes are only Raman active, and the two B_1 modes are silent modes (neither Raman nor IR active). The polar A_1 and E_1 modes split into TO and LO phonon modes with different frequencies due to the macroscopic electric field associated with the longitudinal modes. In the case of GaN the electrostatic forces predominate over the anisotropic short-range forces. Therefore, the TO-LO splitting is larger than the A_1–E_1 splitting.[22] For the lattice vibrations with A_1 and E_1 symmetry, the atomic displacement is parallel and perpendicular to the optical c axis, respectively (see Fig. 1(a)). In case of a uniaxial crystal and arbitrary direction of the phonon wavevector, phonons can be differentiated into ordinary and extraordinary ones with atomic displacement vectors lying either perpendicularly to or in the plane spanned by the phonon wavevector and the optical axis, respectively. Further, the atomic displacement vectors of the extraordinary phonons can be decomposed in transverse and longitudinal components with respect to the phonon wavevector which is illustrated in Fig. 1(a). Thus, phonons with wavevector angles between 0° and 90° to the c axis have mixed A_1–E_1 character. Figure 1(b) shows the directional dispersion of the extraordinary phonon modes. The ordinary phonon with symmetry E_1 and the $E_{2,high}$ phonons have no directional dispersion. The other $E_{2,low}$ phonon at 144 cm^{-1} is not shown here.

B. Raman scattering efficiencies

The Raman scattering efficiency per unit angle $\frac{dS}{d\Omega}$ of the phonons travelling the distance L in the crystal through the volume V can be written according to Mills and Burstein[25]

$$\frac{dS}{d\Omega} = \left(\frac{\omega_s}{c}\right)^4 VL \left| \left\langle 1 + n_\omega \left| \sum_{\mu,\nu=1}^{3} e_\mu^S \delta\chi_{\mu\nu} e_\nu^L \right| n_\omega \right\rangle \right|^2, \quad (1)$$

where $\vec{e}^L(\vec{e}^S)$ are the unit vectors in the direction of polarization of the incident (scattered) light, respectively. The value inside the absolute value signs is the matrix element of an operator between the state with n_ω phonons of frequency ω present and the state with $n_\omega + 1$ phonons describing a Stokes scattering process. Thus, the scattered photon emerges with frequency ω_s, less than that of the incident photon by the small amount ω. $n_\omega = 1/[\exp(\hbar\omega/kT) - 1]$ is the Bose-Einstein factor.

First, we consider the three polar phonon modes of hexagonal crystals with point group C_{6v} which are Raman as well as infrared active. Their Raman scattering intensity depends on the changes $\delta\chi$ of the polarizability tensor elements with contributions of the normal coordinates and the electric field components

$$\delta\chi_{ij}^N = \frac{\partial\chi_{ij}}{\partial Q_N} Q_N + \frac{\partial\chi_{ij}}{\partial E_N} E_N = \sum_{\alpha=1}^{3} \left[\frac{\partial\chi_{ij}}{\partial Q_\alpha} \frac{\partial Q_\alpha}{\partial Q_N} \times \left(1 + \frac{\omega_{TO,\alpha}^2 - \omega^2}{C_{\alpha,ij}^{FH} \omega_{TO,\alpha}^2} \right) \right] \times Q_N. \quad (2)$$

A detailed derivation of the Raman scattering efficiency in wurtzite-type crystals is provided in the work by Irmer *et al.*[24] The letter N denotes the ordinary transverse, extraordinary transverse and the extraordinary longitudinal phonon with the normal coordinates Q_{To}, Q_{Te}, Q_{Le} and the electric fields E_{To}, E_{Te}, E_{Le}, respectively. α numbers the cartesian

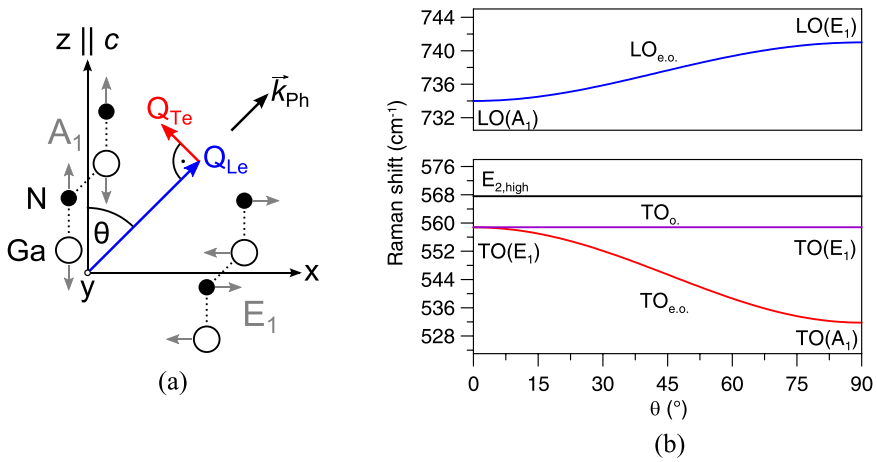

FIG. 1. Phonon modes of α-GaN. (a) The atomic displacement of the lattice vibrations with A_1 and E_1 symmetry is parallel and perpendicular to the optical c axis, respectively. In case of an arbitrary direction of the phonon wavevector $\vec{k}_{Ph}$, the atomic displacement vectors of the extraordinary polar phonons can be decomposed in parts parallel (extraordinary longitudinal) and perpendicular (extraordinary transverse) to the wavevector. Extraordinary phonons those wavevectors include angles θ between 0° and 90° to the c axis have mixed A_1–E_1 character. (b) The directional dispersion of the extraordinary polar modes as function of the angle θ between the phonon wavevector and the c axis of the crystal is shown. The dispersion $\omega(\theta)$ can be obtained by solving the equation $\varepsilon_{\infty\perp} \sin^2\theta(\omega_{LO,E1}^2 - \omega^2)(\omega_{TO,A1}^2 - \omega^2) + \varepsilon_{\infty\parallel} \cos^2\theta(\omega_{LO,A1}^2 - \omega^2)(\omega_{TO,E1}^2 - \omega^2) = 0$ (see, e.g., Eqs. (4)–(40) in Claus *et al.*[23] or Eq. (14) in Irmer *et al.*[24] in the limit of large values k).

coordinates x, y, and z. $\omega_{\mathrm{TO},1} = \omega_{\mathrm{TO},2} = \omega_{\mathrm{TO,E1}}$ $(\omega_{\mathrm{TO},3} = \omega_{\mathrm{TO,A1}})$ indicates the frequency of the transverse phonon polarized in the (x, y) plane (parallel to the z axis). The relation between E_N and Q_N follows from the Born-Huang equations.[24] In Eq. (2) we introduced the Faust-Henry coefficients $C^{FH}_{\alpha,ij}$[15,26]

$$C^{FH}_{\alpha,ij} = \frac{\sqrt{\varepsilon_0(\varepsilon_{s\alpha} - \varepsilon_{\infty\alpha})}}{\omega_{\mathrm{TO},\alpha}} \times \frac{\left(\frac{\partial \chi_{ij}}{\partial Q_\alpha}\right)}{\left(\frac{\partial \chi_{ij}}{\partial E_\alpha}\right)}, \tag{3}$$

where $\varepsilon_{s1} = \varepsilon_{s2} = \varepsilon_{s\perp}$ $(\varepsilon_{\infty 1} = \varepsilon_{\infty 2} = \varepsilon_{\infty\perp})$ denotes the static (high-frequency) dielectric constant in the (x, y) plane, and $\varepsilon_{s3} = \varepsilon_{s\parallel}$ $(\varepsilon_{\infty 3} = \varepsilon_{\infty\parallel})$ the static (high-frequency) dielectric constant parallel to the z axis. According to the symmetry of the tensors, three different Faust-Henry coefficients will appear. We decompose the normal coordinates Q_N in the coordinates Q_α introducing the angles φ and θ which define the direction of the phonon wavevector $\vec{k}_{\mathrm{Ph}} = k_{\mathrm{Ph}}$ $(\sin\theta\cos\varphi, \sin\theta\sin\varphi, \cos\theta)$. The direction of the three normal coordinates $\vec{Q}_{\mathrm{To}} \perp \vec{Q}_{\mathrm{Te}} \perp \vec{Q}_{\mathrm{Le}}$ is given by $\vec{Q}_{\mathrm{To}} \perp (z\,\mathrm{axis}, \vec{k})$, $\vec{Q}_{\mathrm{Te}} \perp (\vec{k}, \vec{Q}_{\mathrm{To}})$, and $\vec{Q}_{\mathrm{Le}} \parallel \vec{k}$. The Raman scattering intensity can now be written as

$$I_{\mathrm{N}}(\omega) = \left(\frac{\omega_s}{c}\right)^4 VL|\vec{e}^{\,\mathrm{S}} \cdot \tilde{R}_{\mathrm{N}} \cdot \vec{e}^{\,\mathrm{L}}|^2 |\langle 1 + n_\omega | Q_{\mathrm{N}} | n_\omega \rangle|^2. \tag{4}$$

The Raman tensors $\tilde{R}_{\mathrm{N}}$ for the polar phonon modes in hexagonal crystals with point group C_{6v} have the form which has been published by several authors. We refer to the table in Claus *et al.*,[23] where some errors appearing in older tables have been corrected. The three matrices $\tilde{R}_{\mathrm{N}}$ for the ordinary transverse phonon $(N = \mathrm{To})$, extraordinary transverse phonon $(N = \mathrm{Te})$, and extraordinary longitudinal phonon $(N = \mathrm{Le})$ are

$$\tilde{R}_{\mathrm{To}} = C \begin{pmatrix} 0 & 0 & -\sin\varphi \\ 0 & 0 & \cos\varphi \\ -\sin\varphi & \cos\varphi & 0 \end{pmatrix}, \tag{5}$$

$$\tilde{R}_{\mathrm{Te}} = \begin{pmatrix} A\sin\theta & 0 & -C\cos\theta\cos\varphi \\ 0 & A\sin\theta & -C\cos\theta\sin\varphi \\ -C\cos\theta\cos\varphi & -C\cos\theta\sin\varphi & B\sin\theta \end{pmatrix}, \tag{6}$$

and

$$\tilde{R}_{\mathrm{Le}} = \begin{pmatrix} A\cos\theta & 0 & C\sin\theta\cos\varphi \\ 0 & A\cos\theta & C\sin\theta\sin\varphi \\ C\sin\theta\cos\varphi & C\sin\theta\sin\varphi & B\cos\theta \end{pmatrix}, \tag{7}$$

with $C(\omega) = c_{\mathrm{TO}}\left(1 + \frac{\omega^2_{\mathrm{TO,E1}} - \omega^2}{C^{\mathrm{FH}}_c \omega^2_{\mathrm{TO,E1}}}\right)$, $A(\omega) = a_{\mathrm{TO}}\left(1 + \frac{\omega^2_{\mathrm{TO,A1}} - \omega^2}{C^{\mathrm{FH}}_a \omega^2_{\mathrm{TO,A1}}}\right)$, and $B(\omega) = b_{\mathrm{TO}}\left(1 + \frac{\omega^2_{\mathrm{TO,A1}} - \omega^2}{C^{\mathrm{FH}}_b \omega^2_{\mathrm{TO,A1}}}\right)$. In the limit of $\omega \to \omega_{\mathrm{TO}}$, the coefficients $A(\omega), B(\omega)$, and $C(\omega)$ result in the Raman tensor elements $a_{\mathrm{TO}}, b_{\mathrm{TO}}$, and c_{TO}.

Equation (4) describes the Raman scattering intensity of phonons (180° backscattering, 90° scattering geometry or near-forward scattering) as well as polaritons (near-forward scattering). In the following, we confine ourselves to the case of phonons (large wavevectors). The matrix elements in Eq. (4) are then $|\langle 1 + n_\omega | Q_N | n_\omega \rangle|^2 = \frac{\hbar(1+n_\omega)}{2V\omega}$. Results for calculation of the matrix elements for polaritons are given in the Appendix. For angles in the range $\theta = 0° \ldots 90°$ the symmetry of the extraordinary TO- and LO-phonons is of mixed character, see Fig. 1. However, for the angles $\theta = 0°$ and $\theta = 90°$ the phonons can be assigned to the following symmetries: The ordinary TO-phonons have symmetry E_1 with polarization in the (x, y) plane independent of the angle θ. The extraordinary TO-phonons have symmetry E_1 for $\theta = 0°$ with polarization in the (x, y) plane and symmetry A_1 for $\theta = 90°$ with polarization in direction z. The Raman tensors are then

$$\begin{aligned} E_1(\mathrm{TO}) : -\tilde{R}_{\mathrm{To}}(\varphi = 90°) &= -\tilde{R}_{\mathrm{Te}}(\theta = 0°, \varphi = 0°) \\ &= \frac{\partial \chi}{\partial Q_x} = \begin{pmatrix} & & c_{\mathrm{TO}} \\ & & \\ c_{\mathrm{TO}} & & \end{pmatrix}, \\ \tilde{R}_{\mathrm{To}}(\varphi = 0°) &= -\tilde{R}_{\mathrm{Te}}(\theta = 0°, \varphi = 90°) \\ &= \frac{\partial \chi}{\partial Q_y} = \begin{pmatrix} & & \\ & & c_{\mathrm{TO}} \\ & c_{\mathrm{TO}} & \end{pmatrix} \\ A_1(\mathrm{TO}) : \tilde{R}_{\mathrm{Te}}(\theta = 90°) &= \frac{\partial \chi}{\partial Q_z} = \begin{pmatrix} a_{\mathrm{TO}} & & \\ & a_{\mathrm{TO}} & \\ & & b_{\mathrm{TO}} \end{pmatrix}. \end{aligned} \tag{8}$$

The extraordinary LO-phonons have symmetry A_1 with polarization in direction z for $\theta = 0°$ and symmetry E_1 with polarization in the (x, y) plane for $\theta = 90°$. The Raman tensors are

$$\begin{aligned} E_1(\mathrm{LO}) : \tilde{R}_{\mathrm{Le}}(\theta = 90°, \varphi = 0°) &= \begin{pmatrix} & & c_{\mathrm{LO}} \\ & & \\ c_{\mathrm{LO}} & & \end{pmatrix}, \\ \tilde{R}_{\mathrm{Le}}(\theta = 90°, \varphi = 90°) &= \begin{pmatrix} & & \\ & & c_{\mathrm{LO}} \\ & c_{\mathrm{LO}} & \end{pmatrix} \\ A_1(\mathrm{LO}) : \tilde{R}_{\mathrm{Le}}(\theta = 0°) &= \begin{pmatrix} a_{\mathrm{LO}} & & \\ & a_{\mathrm{LO}} & \\ & & b_{\mathrm{LO}} \end{pmatrix}. \end{aligned} \tag{9}$$

Due to the macroscopic electric field accompanying the LO-phonons, their Raman tensor elements are different from the TO-phonon ones. The tensor elements are related by

$$\begin{aligned} a_{\mathrm{LO}} &= a_{\mathrm{TO}}\left(1 + \frac{\omega^2_{\mathrm{TO,A1}} - \omega^2_{\mathrm{LO,A1}}}{C^{FH}_a \omega^2_{\mathrm{TO,A1}}}\right) \\ b_{\mathrm{LO}} &= b_{\mathrm{TO}}\left(1 + \frac{\omega^2_{\mathrm{TO,A1}} - \omega^2_{\mathrm{LO,A1}}}{C^{FH}_b \omega^2_{\mathrm{TO,A1}}}\right) \\ c_{\mathrm{LO}} &= c_{\mathrm{TO}}\left(1 + \frac{\omega^2_{\mathrm{TO,E1}} - \omega^2_{\mathrm{LO,E1}}}{C^{FH}_c \omega^2_{\mathrm{TO,E1}}}\right). \end{aligned} \tag{10}$$

The Faust-Henry coefficients can be obtained by measurement of the Raman scattering intensities I_{LO} and I_{TO} of the corresponding LO- and TO-phonons in an undoped crystal

$$\frac{I_{LO}}{I_{TO}} = \frac{(\omega_L - \omega_{LO})^4}{(\omega_L - \omega_{TO})^4} \times \frac{\omega_{TO}}{\omega_{LO}} \times \frac{n(\omega_{LO}) + 1}{n(\omega_{TO}) + 1} \times \left| 1 + \frac{\omega_{TO}^2 - \omega_{LO}^2}{C_\alpha^{FH} \omega_{TO}^2} \right|^2, \quad (11)$$

where ω_L refers to the frequency of the exciting laser expressed in cm^{-1}. For completeness we present the Raman tensors for the nonpolar phonons with E_2 symmetry

$$E_2: \quad \tilde{R}_{E_2}^{(1)} = \begin{pmatrix} & -d & \\ -d & & \\ & & \end{pmatrix}, \quad \tilde{R}_{E_2}^{(2)} = \begin{pmatrix} d & & \\ & -d & \\ & & \end{pmatrix}. \quad (12)$$

In order to ascertain the scattering efficiency of this twofold degenerated phonon mode, the contributions of both Raman tensors given in Eq. (12) have been added

$$|\vec{e}^S \cdot \tilde{R}_{E_2} \cdot \vec{e}^L|^2 = |\vec{e}^S \cdot \tilde{R}_{E_2}^{(1)} \cdot \vec{e}^L|^2 + |\vec{e}^S \cdot \tilde{R}_{E_2}^{(2)} \cdot \vec{e}^L|^2. \quad (13)$$

The scattering intensity of the E_2 phonon does not depend on the phonon wavevector. Therefore, and due to its strong intensity it is suitable as reference phonon for normalization of the Raman spectra. The calculation of the Raman scattering intensity according to Eq. (4) with the Raman tensors defined in Eqs. (5)–(7) requires, as input data, the directions of the polarization vectors and the phonon wavevector. As previously mentioned, the direction of the phonon wavevector $\vec{k}_{Ph}$ can be described by the angle θ between $\vec{k}_{Ph}$ and the z axis and the angle φ between the orthogonal projection of $\vec{k}_{Ph}$ on the (x, y) plane and the x axis.

Table I shows scattering configurations used in this work enabling the measurement of the Raman intensity of all allowed optical phonons of wurtzite-type GaN. The scattering configurations are given according to the Porto notation.[27] $x(zx)y$, for instance, means (from left to right) propagation of the exciting laser light parallel to the x axis of the crystal, z and x refer to the direction of the polarization vectors of incident and scattered light, respectively, and y indicates the direction of the wavevector of the scattered light. The determination of all Raman tensor elements requires 180°, 90°, and 0° scattering experiments.

III. EXPERIMENT

In order to determine the Raman scattering efficiency of all optical phonons accessible in α-GaN, various scattering geometry configurations are necessary to be measured. Many phonons are detectable in 180° backscattering geometry, the LO(E_1) phonon in 90° geometry and the Raman tensor element b_{LO} of the LO(A_1) phonon only in near-forward scattering geometry. Four scattering geometry arrangements used are shown in Fig. 2. In Table I the scattering configurations as well as the corresponding contribution of the Raman tensor elements are summarized. For the scattering process inside (index "i") the crystal wavevector conservation requires $\vec{k}_{iL} = \vec{k}_{iS} + \vec{k}_{Ph}$ and energy conservation requires $\hbar\omega_L = \hbar\omega_S + \hbar\omega_{Ph}$. $\vec{k}_{Ph}$ refers to a wavevector of the phonon excited in a Stokes process and ω_{Ph} to its energy expressed in cm^{-1}.

Most Raman spectra were obtained at room temperature, some backscattering experiments were performed in a temperature range T = 80 K–380 K. The lateral dimensions of a typical α-GaN single crystal investigated in this work were $5 \times 5\,mm^2$. The thickness of this c plane GaN sample was about 1 mm.

TABLE I. Allowed Raman tensor elements for different scattering configurations which are given with respect to the Porto notation. θ refers to the included angle between phonon wavevector $\vec{k}_{Ph}$ and z axis. x: [100], y: [010], z: [001], u: [011], and v: [01$\bar{1}$].

Scattering configuration	Angle θ	Contribution of Raman tensor elements
180° scattering geometry		
$z(yy)\bar{z}$, $z(xx)\bar{z}$	0°	$a_{LO}^2 + d^2$
$z(yx)\bar{z}$, $z(xy)\bar{z}$	0°	d^2
$x(yy)\bar{x}$	90°	$a_{TO}^2 + d^2$
$x(yz)\bar{x}$, $x(zy)\bar{x}$	90°	c_{TO}^2
$x(zz)\bar{x}$	90°	b_{TO}^2
$x(uu)\bar{x}$	90°	$1/4(a_{TO} + b_{TO})^2 + c_{TO}^2 + 1/4d^2$
$x(uv)\bar{x}$	90°	$1/4(a_{TO} - b_{TO})^2 + 1/4d^2$
90° scattering geometry		
$y(zz)x$	90°	b_{TO}^2
$y(zy)x$, $y(xz)x$	90°	$1/2c_{TO}^2 + 1/2c_{LO}^2$
$y(xy)x$	90°	d^2
0° scattering geometry		
$x(zz)x$	θ	$b_{LO}^2 \cos^2\theta + b_{TO}^2 \sin^2\theta$
$x(zy)x$, $x(yz)x$	θ	c_{TO}^2
$x(yy)x$	θ	$a_{LO}^2 \cos^2\theta + a_{TO}^2 \sin^2\theta + d^2$
$x(uz)x$, $x(zu)x$	θ	$1/2b_{LO}^2 \cos^2\theta + 1/2c_{TO}^2 + 1/2b_{TO}^2 \sin^2\theta$
$x(uy)x$, $x(yu)x$	θ	$1/2a_{LO}^2 \cos^2\theta + 1/2c_{TO}^2 + 1/2a_{TO}^2 \sin^2\theta + 1/2d^2$
$x(uu)x$	θ	$1/4(a_{LO} + b_{LO})^2 \cos^2\theta + c_{TO}^2 + 1/4(a_{TO} + b_{TO})^2 \sin^2\theta + 1/4d^2$
$x(uv)x$	θ	$1/4(a_{LO} - b_{LO})^2 \cos^2\theta + 1/4(a_{TO} - b_{TO})^2 \sin^2\theta + 1/4d^2$

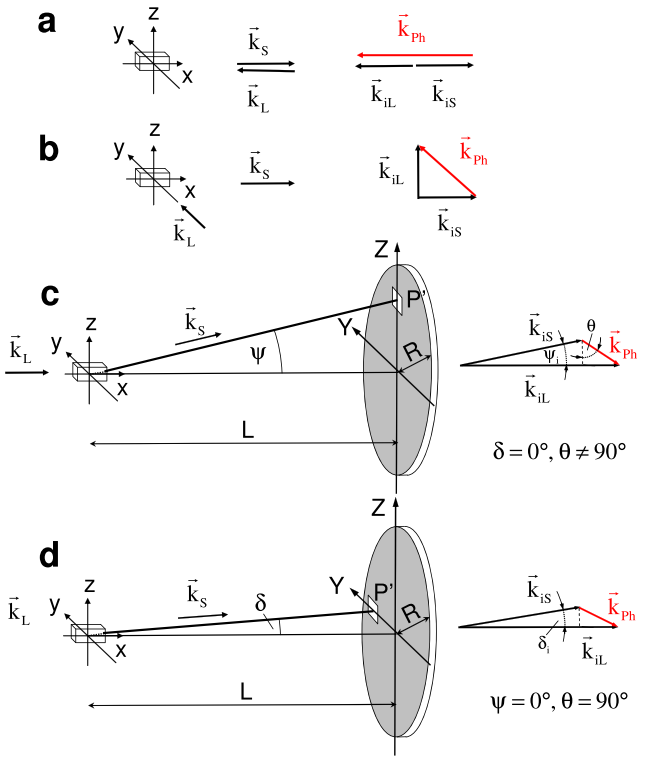

FIG. 2. Scattering configurations and transferred phonon wavevector: (a) 180° scattering (backscattering), (b) 90° scattering, (c) 0° scattering (near-forward scattering) in the (x, z) plane, (d) 0° scattering (near-forward scattering) in the (x, y) plane. $\vec{k}_L$ and $\vec{k}_S$ denote the wavevectors of the laser light and scattered light, respectively. $\vec{k}_{Ph}$ refers to the phonon wavevector. The index "i" indicates the corresponding values inside the crystal.

A. 180° scattering

Raman measurements were conducted using a Labram HR 800 Raman spectrometer with a piezoelectrically cooled charge-coupled device (CCD) detector. The spectra were excited applying the 532 nm (2.33 eV) line of a frequency-doubled Nd:YAG laser at a power level of about 10 mW at the sample. By passing the linearly polarized laser light through an Olympus microscope objective, the laser beam was focused on the sample surface. The scattered light was collected by the same objective and its polarization was analyzed. The laser polarization was changed with a half-wave quartz plate that rotates the linear polarization axis by 90°. A rotatable quartz waveplate behind the analyzer realizes the respective rotation of the polarization axis in the direction with maximum sensitivity of the spectrometer. In Fig. 2(a) the scattering configuration is depicted with the propagation direction of the exciting laser light and the scattered light along the x axis. Thus, the electric field of incident and scattered light was polarized in the (y, z) plane. If the GaN sample is positioned beneath the microscope with its c axis parallel to the z axis of the laboratory coordinate system an angle $\theta = 90°$ between phonon wavevector and c axis is realized. Other backscattering measurements were performed with the c axis oriented parallel to the x axis.

B. 90° scattering

In Fig. 2(b) the 90° scattering arrangement is shown. Raman spectra were obtained using a T 64 000 Raman spectrometer (Horiba, Jobin Yvon). The GaN sample was positioned in the macro chamber with its c axis oriented parallel to the z axis of the laboratory coordinate system. The spectra were excited applying the 514.5 nm (2.41 eV) line of an Ar^+-laser at a power level of about 100 mW at the sample. After passing the spectrometer equipped with gratings of 1800 grooves/mm in subtractive mode, the scattered light was analyzed by a LN cooled CCD detector. By means of a polarization rotator the laser beam polarization could be changed from (i) parallel to the z axis to (ii) parallel to the x axis. The scattered light was analyzed with polarization parallel or perpendicular to the z axis using an analyzer positioned in the parallel light path between sample and entrance slit of the spectrometer. The polarization dependence of the spectrometer was compensated using a half-wave quartz plate.

C. Near-forward scattering

Special care has to be taken in case of nearly forward scattering whose scattering configurations are illustrated in Figs. 2(c) and 2(d). Both, laser beam and sample were thoroughly adjusted in order to avoid the capture of laser light into the spectrometer. The laser beam leaving the sample was masked in the centre of the entrance lens of the imaging system. Furthermore, care is necessary to avoid gathering of scattered light excited by the laser beam partly backscattered at the inner crystal surface. As in the case of 90° scattering, the 514.5 nm line of the exciting Ar^+-laser was used and the sample was mounted in the macro chamber of the spectrometer T 64 000. The exciting laser beam directed along the x axis was focused onto the sample by a laser objective. The scattered light enters the spectrometer through a small rectangular window at P' in front of the entrance lens. The window position can be shifted along the Z axis (Fig. 2(c)) or along the Y axis (Fig. 2(d)). In this way, scattered light originating from scattering processes with defined, different wavevectors can be observed and in the case of varying the window position along the Z axis also different angles θ.

Since there is an excellent agreement with our experimental data the following parameters were adopted in this work and used for the calculations:

$\varepsilon_{\infty\perp} = 5.14$, $\varepsilon_{\infty\parallel} = 5.31$ (Ref. 28)
$\omega_{TO,A1} = 531.8\,cm^{-1}$, $\omega_{TO,E1} = 558.8\,cm^{-1}$,
$\omega_{E2,high} = 567.6\,cm^{-1}$, $\omega_{E2,low} = 144\,cm^{-1}$,
$\omega_{LO,A1} = 734\,cm^{-1}$, $\omega_{LO,E1} = 741\,cm^{-1}$. (Ref. 29)

IV. EXPERIMENTAL RESULTS

A. 180° scattering

The intensities of the corresponding scattering configurations listed in Table I depend on the Raman tensor elements a_{TO}, a_{LO}, b_{TO}, c_{TO}, and d. Comparing both configurations $x(uu)\bar{x}$ and $x(vv)\bar{x}$, we obtained the sign $a_{TO}/b_{TO} < 0$. This is not shown here. Instead, we discuss in more detail the determination of the Raman scattering cross-section of both, the A_1(TO) and the A_1(LO) phonon, as well as the Faust-Henry coefficient C_a^{FH} connected with them.

Figure 3 shows results of a typical measurement. All spectra were normalized with respect to the strong and narrow non-polar $E_{2,high}$ phonon mode.[30]

The Raman scattering intensities were determined as areas under the phonon bands, the areas were numerically integrated. In some cases, the phonons were fitted by a sum of Lorentz-, asymmetric Lorentz- or Voigt-functions. This works well in separating the bands to be measured from weak spurious phonon bands forbidden according to the selection rules, because all phonon bands are more or less asymmetric as shown in Fig. 4. In order to exclude a possible contribution of two-phonon modes, we performed measurements as a function of temperature in the range 80 K–380 K. Due to the different temperature dependence of one-phonon and two-phonon processes the contribution of the latter should be negligible at low temperatures. However, the asymmetry can also be observed at low temperatures, see Fig. 4.

B. 90° scattering

The measurement of the $E_1(LO)$ phonon is possible using a 90° scattering arrangement. Figure 5 shows typical spectra of an α-GaN single crystal obtained in the configuration (b) of Fig. 2. In this case the wavevectors of incident and scattered light are $\vec{k}_L = k_L(0,1,0)$ and $\vec{k}_S = k_S(1,0,0)$ and the phonon wavevector is $\vec{k}_{Ph} = \vec{k}_L - \vec{k}_S \approx k_{Ph}/\sqrt{2}\ (-1,1,0)$ due to $k_S \approx k_L$, the angles are $\varphi = 135°$ and $\theta = 90°$. For the polarization configuration (zy) the polarization vectors are $\vec{e}^{\,L} = (0,0,1)$ and $\vec{e}^{\,S} = (0,1,0)$. With $\omega = \omega_{TO,E1}$ in Eq. (5)

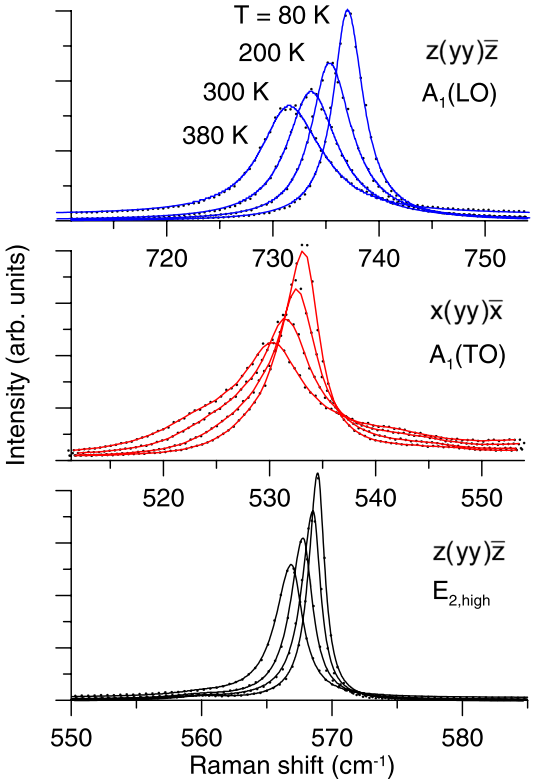

FIG. 4. Profiles of phonon bands as function of the temperature. The Raman spectra recorded in backscattering of the $A_1(LO)$ and $A_1(TO)$ phonons were normalized with respect to the $E_{2,high}$ phonon intensity obtained in $z(yy)\bar{z}$ and $x(yy)\bar{x}$ configuration, respectively.

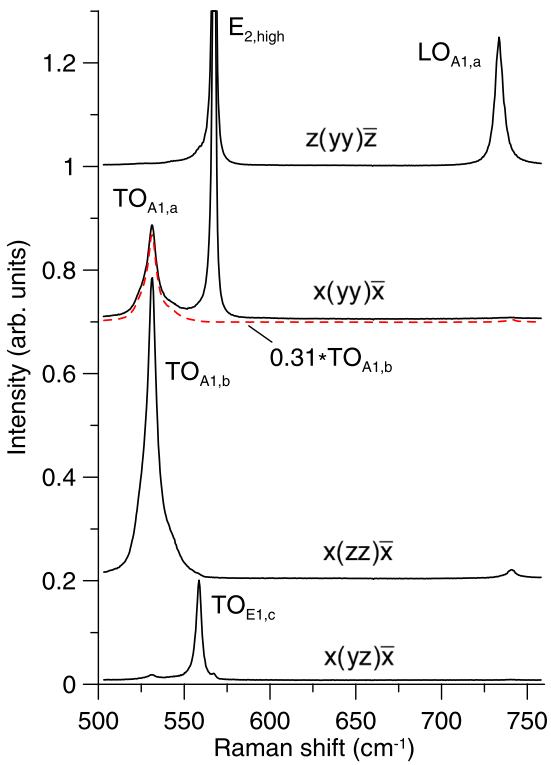

FIG. 3. Raman spectra of a α-GaN single crystal recorded in backscattering geometry (i) in direction z (growth direction) and (ii) from a surface in direction x perpendicular to it. The two letters in brackets indicate the polarization direction of the incident and scattered light, respectively. The spectra were normalized with respect to the $E_{2,high}$ phonon mode and shifted for clarity.

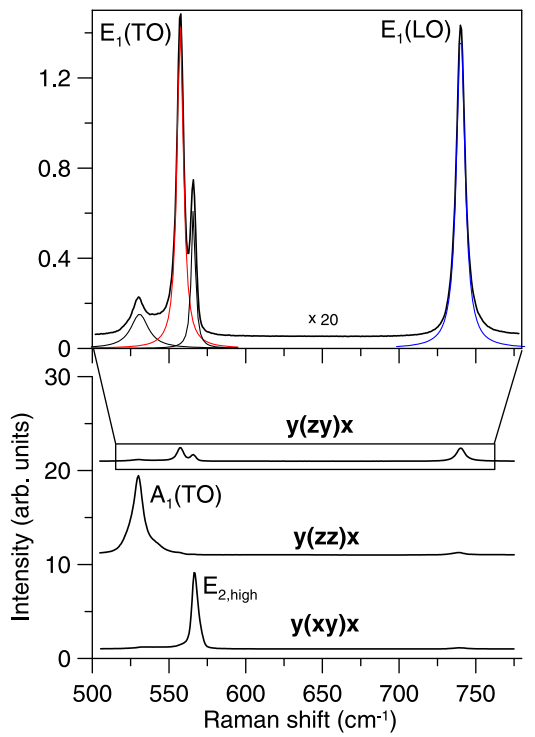

FIG. 5. Raman spectra of a α-GaN crystal recorded in 90° scattering geometry. The spectra were normalized with respect to the $E_{2,high}$ phonon intensity obtained in $y(xy)x$ configuration. All spectra in the lower panel are shifted for clarity. The upper panel shows the experimental data of the $y(zy)x$ configuration and the fit results in more detail, magnification ×20.

TABLE II. Scattering cross-section of α-GaN relative to the $E_{2,high}$ phonon mode.

Raman mode	Raman shift (cm^{-1})	Relative scattering cross-section	Raman tensor element
$E_{2,high}$	567.6	1	$d^2_{E2,high} = 1$
$E_{2,low}$	144	$(0.40\pm0.05)\cdot10^{-2}$	$d^2_{E2,low} = (0.49\pm0.05)\cdot10^{-3}$
A_1(TO)	531.8	0.63 ± 0.02	$a^2_{TO} = 0.58\pm0.02$
		1.98 ± 0.03	$b^2_{TO} = 1.82\pm0.03$
A_1(LO)	734	0.66 ± 0.02	$a^2_{LO} = 0.92\pm0.02$
		2.00 ± 0.03	$b^2_{LO} = 2.78\pm0.03$
E_1(TO)	558.8	0.35 ± 0.02	$c^2_{TO} = 0.34\pm0.02$
E_1(LO)	741	0.43 ± 0.02	$c^2_{LO} = 0.61\pm0.02$

and $\omega = \omega_{LO,E1}$ in Eq. (7) we obtain $|\vec{e}^S\cdot\tilde{R}_{To}\cdot\vec{e}^L|^2 = 1/2c^2_{TO}$ and $|\vec{e}^S\cdot\tilde{R}_{Le}\cdot\vec{e}^L|^2 = 1/2c^2_{LO}$, respectively. The two other expressions are $|\vec{e}^S\cdot\tilde{R}_{Te}\cdot\vec{e}^L|^2 = |\vec{e}^S\cdot\tilde{R}_{E_{2,high}}\cdot\vec{e}^L|^2 = 0$, see Eqs. (6) and (13). For the polarizations (zz) and (xy) the nonvanishing expressions are $|\vec{e}^S\cdot\tilde{R}_{Te}\cdot\vec{e}^L|^2 = b^2_{TO}$ with $\omega = \omega_{TO,A1}$ and $|\vec{e}^S\cdot\tilde{R}_{E_{2,high}}\cdot\vec{e}^L|^2 = d^2$, respectively. In the spectrum $y(zy)x$, the E_1(LO) as well as the E_1(TO) phonon can be observed, whose intensity can be obtained from backscattering measurements as well (see Fig. 3). It should be noted that the determination of the intensity ratio $r_c = I_{LO,E1}/I_{TO,E1}$ requires special care. Small deviations Δ from the exact scattering angle 90° have a strong influence onto the ratio r_c which is given by $r_c(\Delta) = r_c(90°)\sin^2(90°+\Delta)/\ [1-\cos(90°+\Delta)]^2$. The ratio r_c has no extremum at $\Delta = 0$ but diminishes for $\Delta > 0$ and rises for $\Delta < 0$. Therefore the crystal has to be positioned very carefully. The relative intensity $I_{LO,A1}$ presented in Table II is the mean value of 8 measurements with different rectangular single crystals and a change of the crystal orientation by 90° rotating around the z axis.

C. 0° scattering

Raman scattering of the A_1(LO) phonon with the tensor element b_{LO} responsible for it requires the polarization (zz) of the laser/scattered light. A wavevector component in z direction is necessary for observation of the A_1(LO) phonon propagating in z direction. This can be achieved with near-forward scattering in (x, z) plane, for instance (see Fig. 2(c)). Observation is possible with a near-forward scattering in x direction. Assuming $\vec{k}_S \approx \vec{k}_L$ the phonon wavevector would be nearly parallel to the z axis for small angles ψ_i. However, for Stokes scattering due to $k_S = 2\pi n_S/\lambda_S < k_L = 2\pi n_L/\lambda_L$, the phonon wavevector also has components in x direction. Taking the refraction at the crystal boundary into account, the smallest angle θ between the phonon wavevector and the z axis achievable using the laser wavelength 514.5 nm is about 19°. From Table I we see that the intensity of the A_1(LO) phonons measured in the configurations $x(zz)x$ and $x(yy)x$ gives the b^2_{LO}/a^2_{LO} ratio independent of the angle θ. Figure 6 shows spectra measured with different positions of the window P′ on the Z axis of the screen in front of the entrance lens of the spectrometer ($Y = 0$). The scattered light stems from scattering processes inside the crystal with angles ψ_i between the wavevectors k_{iS} and k_{iL}. With decreasing angle ψ_i, the x component of k_{Ph} and the angle θ enlarge. Accordingly, the frequency of the extraordinary LO-phonon shifts and the contribution of the Raman tensor elements with A_1 symmetry diminishes. The configuration $x(zz)x$ allows contributions of the element b_{TO} as well. Due to the small phonon wavevector magnitude in near-forward scattering, extraordinary polaritons with frequencies downshifted from the frequency $\omega_{TO,A1}$ are observed. (Referring to the work of Irmer *et al.*[24] further details are not shown here.) The spectra in Fig. 6 were normalized with respect to the $E_{2,high}$ intensity. In Fig. 7, it is shown that the intensity ratio

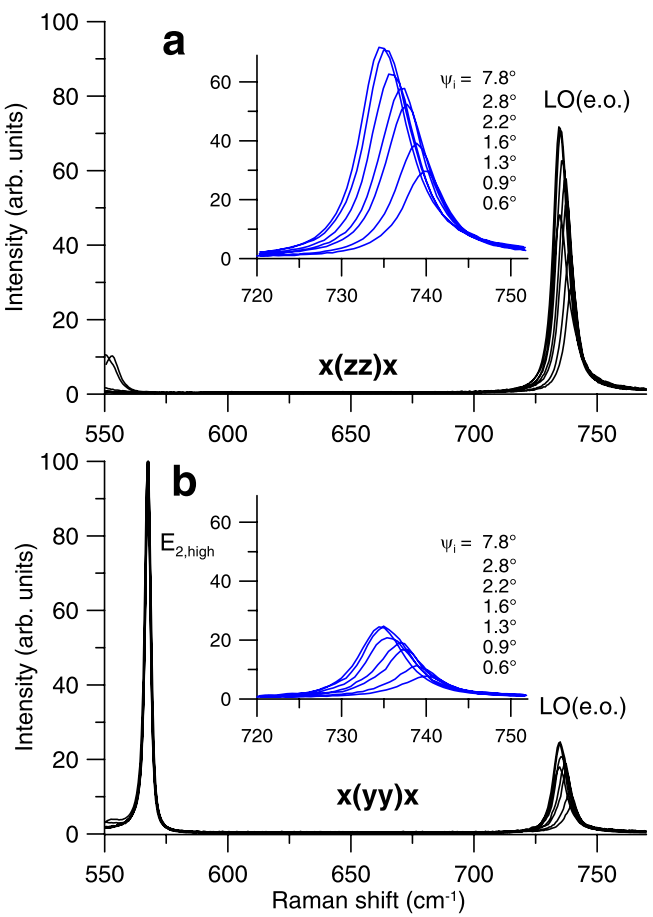

FIG. 6. Raman spectra of the LO(e.o.)-phonon: 0° scattering in the (x, z) plane (see Fig. 2(c)). The spectra are shown as function of the angle ψ_i between incident and scattered light wavevectors k_{iL} and k_{iS}. The spectra were normalized with respect to the $E_{2,high}$ phonon intensity. The Raman tensor elements b_{LO} and a_{LO} are responsible for the scattered intensity of the LO(e.o.)-phonon using the $x(zz)x$ and $x(yy)x$ configurations, respectively.

of the LO(A_1) phonons measured with both polarization, is nearly constant.

D. Faust-Henry coefficients

The Raman scattering intensity data summarized in Table II were used in order to calculate the Faust-Henry coefficients according to Eq. (11).

However, for each coefficient C_α^{FH} two possible solutions can be found. The calculation yields: $C_a^{FH} = \{0.40, -3.46\}$, $C_b^{FH} = \{0.40, -3.81\}$, $C_c^{FH} = \{0.33, -2.31\}$.

The two solutions with different sign correspond to destructive or constructive superposition of the deformation potential scattering and the electrooptical scattering. The measurement of TO phonon-polaritons with near-forward scattering enables one to assign one solution unambiguously. With decreasing wavevector values their frequency ω is shifted from the TO-phonon value towards smaller ones which influences their Raman scattering intensity. In order to calculate the Raman intensity of polaritons, Eqs. (4)–(7) can still be used. However, the calculation of the matrix element in Eq. (4) results in a different expression than used for phonons (see Ref. 24). Because we need polaritons with defined E_1 or A_1 symmetry, near-forward scattering in the (x, y) plane is used with angle $\theta = 90°$ between the polariton wavevector and the c axis of the crystal (see Fig. 2(d)). Figures 8(a), 9(a), and 10(a) show Raman spectra of polaritons measured with different polarizations which filter out the contributions of different Raman tensor elements. Small bands at fixed frequencies can be seen in addition to the polariton spectra. In the case of the extraordinary polaritons this are the TO(A_1) phonons at 531.1 cm^{-1} and in the case of the ordinary polaritons this are the TO(E_1) phonons at 558.9 cm^{-1}. The observed weak bands are not allowed according to the selection rules and stem from 180° scattering processes by reflections inside the crystal. The frequency

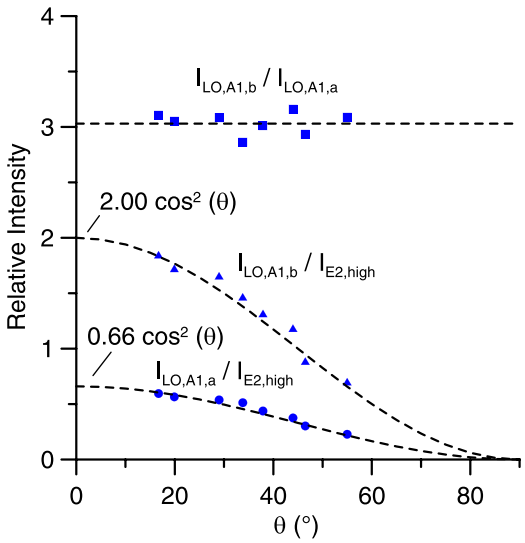

FIG. 7. Intensities of the LO(e.o.)-phonon obtained in the $x(zz)x$ and $x(yy)x$ scattering configuration as function of the angle θ between phonon wavevector and c axis of the α-GaN crystal. The spectra were normalized with respect to the $E_{2,high}$ phonon intensity. 3.03 was obtained as mean value of the ratio of the LO(e.o.)-phonon intensities from the two configurations.

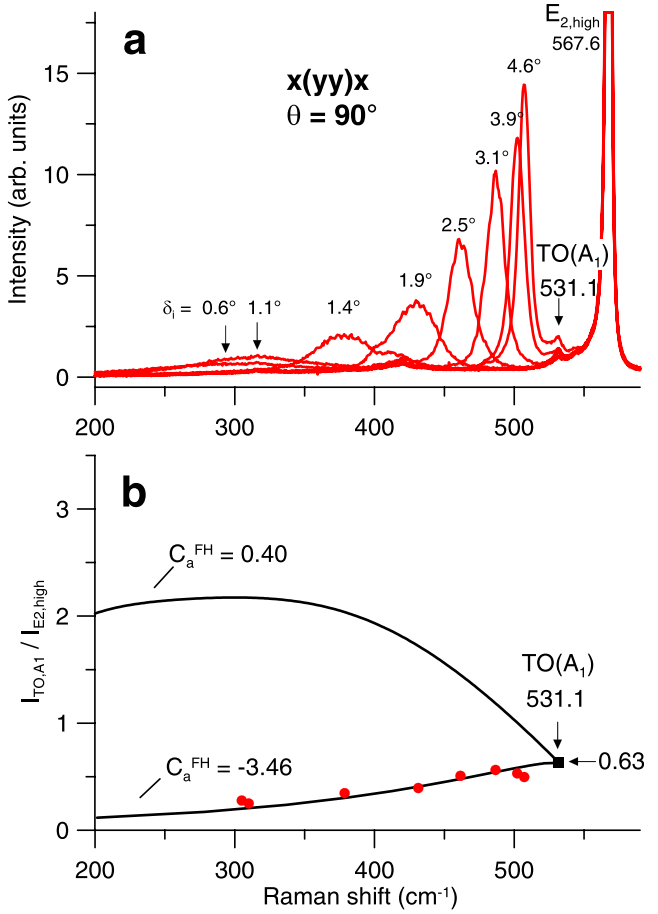

FIG. 8. (a) Raman spectra of the extraordinary polariton, $\theta = 90°$, $x(yy)x$. Near-forward scattering in direction x, scattering in the (x, y) plane, polarization parallel (yy) of the incident and scattered light electrical field vectors. The parameter δ_i is the angle between the wavevectors of incident and scattered light inside the crystal, $\psi_i = 0°$. (b) Polariton Raman efficiency as function of the frequency (full circles). The solid lines indicate calculations using the previously determined Faust-Henry coefficients C_a^{FH}. For $\omega \to \omega_{TO,A1}$ (large k_{Ph}) the branches reach the relative Raman cross-section connected with a_{TO}.

of the LO-phonons in the spectra is fixed to the $\omega_{LO,E1}$ frequency at $\theta = 90°$ (not shown here). Figures 8(b), 9(b), and 10(b) show the measured intensities as function of the frequency (full circles) compared with calculated intensities for the corresponding solutions of the Faust-Henry coefficients (solid lines). The comparison excludes the solutions with the positive sign of the coefficients. Based on our measurements, the three Faust-Henry coefficients are therefore $C_a^{FH} = -3.46$, $C_b^{FH} = -3.81$, and $C_c^{FH} = -2.31$.

Due to most common c plane orientation of α-GaN crystals, the Faust-Henry coefficient C_a^{FH} is most important in order to deduce charge carrier density and mobility from Raman measurements in backscattering geometry. Additionally, we examined the temperature dependence of this Faust-Henry coefficient C_a^{FH} in the range T = 80 K–380 K. In Fig. 11 the value of C_a^{FH} as function of the temperature is depicted.

E. Raman tensor elements

Conclusions from Raman scattering intensities on Raman tensor elements require accounting for the

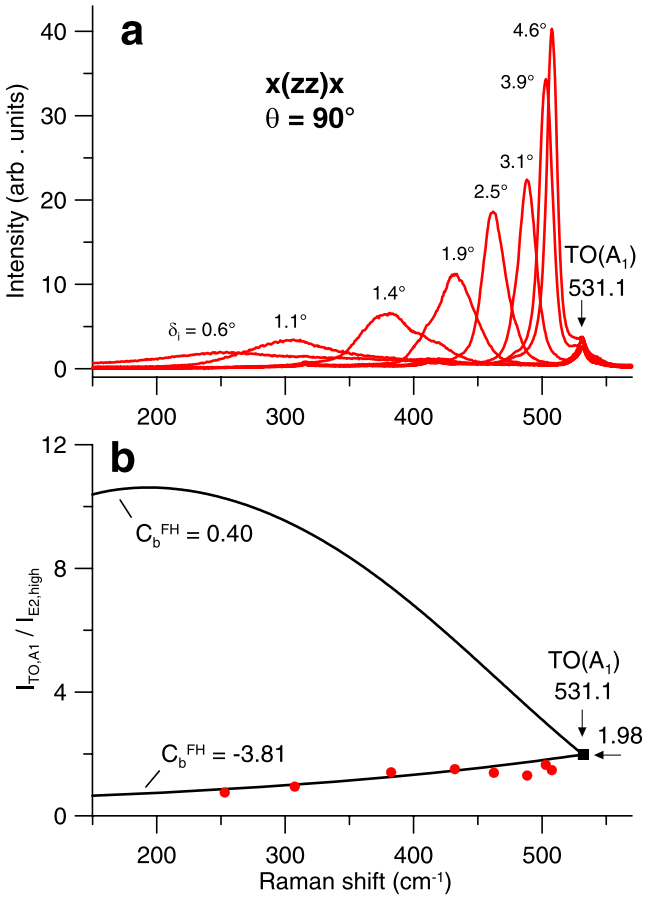

FIG. 9. (a) Raman spectra of the extraordinary polariton, $\theta = 90°$, $x(zz)x$. Near-forward scattering in direction x, scattering in the (x, y) plane, polarization parallel (zz) of the incident and scattered light electrical field vectors. The parameter δ_i is the angle between the wavevectors of incident and scattered light inside the crystal, $\psi_i = 0°$. (b) Polariton Raman efficiency as function of the frequency (full circles). The solid lines indicate calculations using the previously determined Faust-Henry coefficient C_b^{FH}. In the limit $\omega \to \omega_{TO,A1}$ the square refers to the relative Raman cross-section connected with b_{TO}. The intensities $I_{E2,high}$ were measured in the configuration $x(yy)x$.

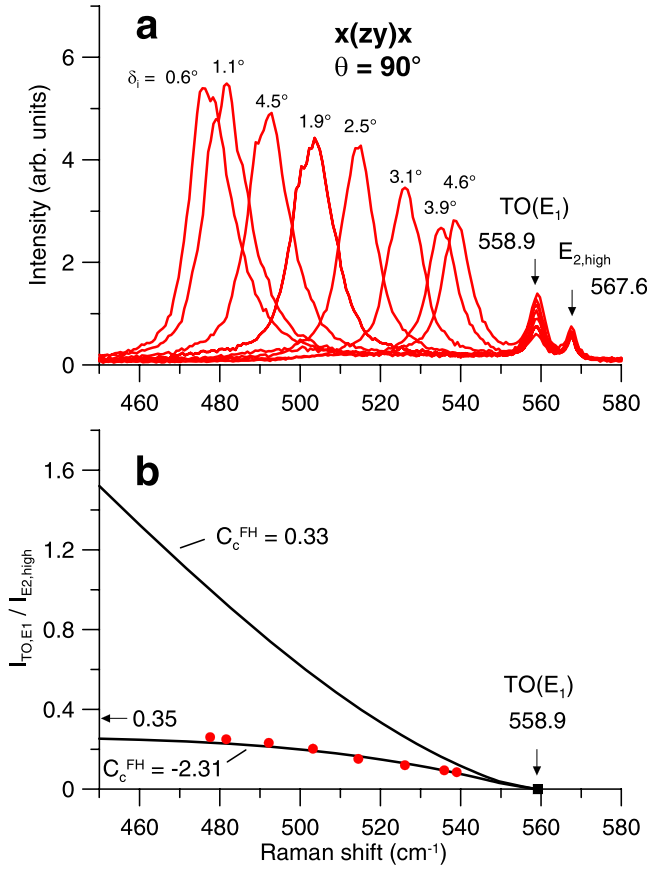

FIG. 10. (a) Raman spectra of the ordinary polariton, $\theta = 90°$, $x(zy)x$. Near-forward scattering in direction x, scattering in the (x, y) plane, crossed polarization (zy) of the incident and scattered light electrical field vectors. The parameter δ_i is the angle between the wavevectors of incident and scattered light inside the crystal, $\psi_i = 0°$. (b) Polariton Raman efficiency as function of the frequency. The solid lines indicate the theoretical calculation using the previously determined Faust-Henry coefficient C_c^{FH}. In the limit $\delta_i \to 0$ the low branch converges to the relative Raman cross-section connected with c_{TO}. The intensities $I_{E2,high}$ were measured in the configuration $x(yy)x$.

dependence of the scattering cross-sections on the phonon frequencies. In order to determine the Raman tensor elements of the TO-phonons relative to the one of the $E_{2,high}$ phonon mode we used the following expression similar to Eq. (11):

$$t_l^2 = \frac{(\omega_L - \omega_{E2,high})^4}{(\omega_L - \omega_l)^4} \times \frac{\omega_l}{\omega_{E2,high}} \times \frac{n(\omega_{E2,high}) + 1}{n(\omega_l) + 1} \times \frac{I_l}{I_{E2,high}} \times d_{E2,high}^2, \quad (14)$$

where l numbers the Raman tensor element $t_l = (a_{TO}, b_{TO}, c_{TO})$ and the relative Raman intensity $I_l = (I_{TO,A1}, I_{TO,A1}, I_{TO,E1})$ connected with the contribution of the corresponding Raman tensor element. $\omega_1 = \omega_2 = \omega_{TO,A1}$ $(\omega_3 = \omega_{TO,E1})$ denote the Raman frequencies of the TO-phonon of A_1 (E_1) symmetry.

Following that, the Raman tensor elements of the LO-phonons were calculated using Eq. (10). Relative Raman scattering cross-sections and Raman tensor elements are summarized in Table II. It should be noted that the ratio $I_{LO,A1,b}/I_{LO,A1,a}$ equals b_{LO}^2/a_{LO}^2.

V. DISCUSSION

Among the three Faust-Henry coefficients, C_a^{FH} is the only one that has been used up to now in connection with determination of free carrier concentration and mobility with coupled LO-phonon plasmon modes.[31] Some authors used simple Drude theory for cubic crystals without any Faust-Henry coefficients in order to obtain carrier concentrations from coupled LO-phonon plasmon modes[43–47] or used an empiric equation,[48,49] but this level is suitable only for crude estimations of carrier concentrations.[31] Its value was introduced applying different methods. In the period before its first determination, some authors used the value $C^{FH} = -0.5$ of cubic GaAs.[32,33] Later, in the analysis of coupled LO-phonon plasmon modes C_a^{FH} was simply regarded as a fit parameter and the values 0.4[17,34,35] or 0.48[20,36–38] were used. Measurements based on the determination of $TO(A_1)$ and $LO(A_1)$ phonons gave the values -5.2,[18] -3.8,[19] and 0.52.[39] The values -5.2 and -3.8 were later adopted by other authors.[10,40] Again, it should be emphasized that according to Eq. (11) the same intensity ratio of the corresponding LO-

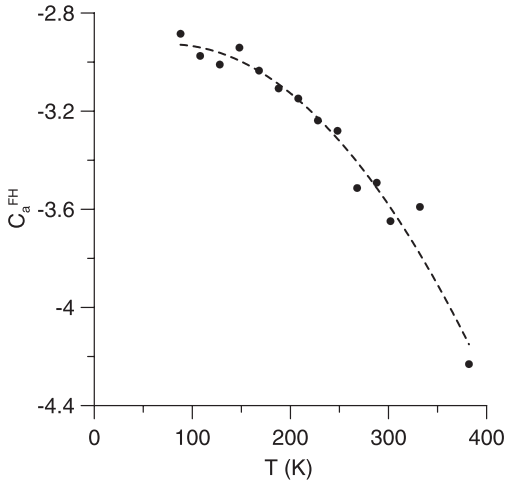

FIG. 11. C_a^{FH} as function of temperature.

and TO-phonons yields two solutions of the associated Faust-Henry coefficient C_α^{FH}. Being aware of that, the literature values of C_a^{FH} are in rather good accordance with one of the two solutions obtained in Sec. IV D. Unfortunately, from measurements of the Raman scattering intensity of LO- and TO-phonons the sign of the Faust-Henry coefficients cannot be concluded in principle.

Reports on measurements of relative or absolute Raman cross-sections of phonons in GaN are scarce in the literature. Loa *et al.*[41] report measurements of absolute and relative efficiencies of the phonons which are accessible with backscattering measurements. Using their values obtained on the sample α-GaN (3.4 μm), the ratio $r_a = I_{\mathrm{LO,A1,a}}(x(yy)\bar{x})/I_{\mathrm{TO,A1,a}}(z(xx)\bar{z}) = 0.43/0.54 = 0.80$ arises. Applying Eq. (11) results in the Faust-Henry coefficient $C_a^{FH} = \{0.43, -9.1\}$.

Better agreement with our own value $r_a = 1.05$ (see Table II) results from comparison with measurements of the relative scattering cross-sections of these phonons performed by other authors. The values $r_a = 1.01$ and $r_a = 0.95$ can be deduced from the C_a^{FH} values reported by Demangeot *et al.*[19] and Wetzel *et al.*,[18] respectively.

Using 180° scattering, Pezzotti *et al.*[42] investigated intensity variations of the polarized Raman bands of E_1(TO), A_1(TO), and E_2 α-GaN phonons as a function of the in-plane rotation angle using the *a* plane of the crystal. However, comparisons between the intensities of the different phonons are not given. From fits of the A_1(TO) phonon intensities as function of the rotation angle they found for the two Raman tensor contributions $a = 0.181$ and $b = -0.859$. This corresponds to an intensity ratio $I_{\mathrm{TO,A1,a}}/I_{\mathrm{TO,A1,b}} = a^2/b^2 = 0.044$ which is much lower than our result 0.32 for this ratio or the value 0.22 calculated with relative intensities given in Ref. 41. A possible reason for the differences could be the fit procedure for A_1(TO) based on an incorrect Eq. (20) in Ref. 42. We get $I^{\parallel}_{\mathrm{TO,A1}} \sim |\vec{e}^{\,\mathrm{S}} \cdot \tilde{R}_{\mathrm{Te}} \cdot \vec{e}^{\,\mathrm{L}}|^2 = (a_{\mathrm{TO}} \cos^2\phi + b_{\mathrm{TO}} \sin^2\phi)^2 = 1/4[(a_{\mathrm{TO}} + b_{\mathrm{TO}}) + (a_{\mathrm{TO}} - b_{\mathrm{TO}}) \cos 2\phi]^2$ if we use $\vec{e}^{\,\mathrm{S}} = \vec{e}^{\,\mathrm{L}} = (0, \cos\phi, \sin\phi)$, $\theta = 90°$ and $\omega_{\mathrm{TO,A1}} = 531.8\,\mathrm{cm}^{-1}$ in Eqs. (4) and (6). This corresponds to the 180° scattering along the *x* axis of an *a* plane oriented crystal (see Fig. 2) where the angle ϕ lies in the *a* plane and is defined as angle between the rotator/analyzer and the *c* axis. Measurements with angles $\phi = 0°$ and $\phi = 90°$ correspond to the configurations $x(yy)\bar{x}$ with $I^{\parallel}_{\mathrm{TO,A1}} \sim a^2_{\mathrm{TO}}$ and $x(zz)\bar{x}$ with $I^{\parallel}_{\mathrm{TO,A1}} \sim b^2_{\mathrm{TO}}$, shown in Fig. 3. Measurements of $I_{\mathrm{TO,A1,a}}$ and $I_{\mathrm{TO,A1,b}}$ are easy to perform with our backscattering configurations $x(yy)\bar{x}$ and $x(zz)\bar{x}$, rotating the sample around the *x* axis by 90°.

Regarding the scattering cross-sections of the E_1(LO) phonon related to the c_{LO} Raman tensor element and the A_1(LO) phonon related to the b_{LO} Raman tensor element we have not found data in the literature.

VI. CONCLUSION

In this study, we determined all Faust-Henry coefficients in α-GaN. Faust-Henry coefficients describe the contributions of the lattice displacements and the electric field associated with them to the Raman scattering efficiency. They give important information about the deformation potential and the electrooptic tensor. In cubic crystals for this aim one Faust-Henry coefficient is sufficient, whereas in wurtzite crystals three coefficients appear. Values of the Faust-Henry coefficients are necessary for the determination of charge carrier concentration and mobility from Raman measurements. Such measurements using the LO-phonon plasmon coupling are widely-used because the Raman measurements are contactless, non-destructive, and with excellent lateral and in the depth resolution. Up to now in the literature exclusively the coefficient C_a^{FH} was determined, with different results and signs. We report new measurements including the temperature dependence of this coefficient. In order to determine the sign unambiguously, we used Raman measurements of the intensity of TO-phonon polariton modes in dependence on their wavevector. In case of α-GaN the obtained Faust-Henry coefficients connected with the corresponding Raman tensor elements are $C_a^{FH} = -3.46$, $C_b^{FH} = -3.81$, and $C_c^{FH} = -2.31$. The coefficient C_a^{FH} is the proper one for analysis of 180° scattering measurements on the commonly used *c* plane GaN, for other orientations the coefficients C_b^{FH} and C_c^{FH} might be necessary. The determination of the coefficients required measurement of the Raman scattering efficiencies of all polar optical phonons. Based on these measurements, the Raman tensors for α-GaN were determined.

ACKNOWLEDGMENTS

The authors gratefully acknowledge the fruitful cooperation with G. Leibiger and F. Habel (Freiberger Compound Materials GmbH), especially in providing high-quality GaN specimens as well as supporting the sample preparation. This work was performed within the Cluster of Excellence "Structure Design of Novel High-Performance Materials via Atomic Design and Defect Engineering (ADDE)" which was financially supported by the European Union (European regional development fund) and by the Ministry of Science and Art of Saxony (SMWK).

APPENDIX: MATRIX ELEMENTS FOR THE POLARITONS

We have three polariton branches with orthogonal atomic displacement vectors $\vec{Q}_{To}$, $\vec{Q}_{Te}$, and $\vec{Q}_{Le}$ of the ordinary transverse, extraordinary transverse, and the extraordinary longitudinal polaritons. The planar modes with atomic displacements $\vec{Q}_x$, $\vec{Q}_y$ in the isotropic (x, y) plane have twofold degenerate symmetry E_1 and the axial modes with displacement $\vec{Q}_z$ in z direction have symmetry A_1.

1. Ordinary mode $\vec{Q}_{\mathrm{To}}$

In the isotropic (x, y) plane the matrix element in Eq. (4) for the degenerate mode with symmetry E_1 yields

$$\begin{aligned}\langle n_\omega+1|\vec{Q}_{\mathrm{To}}|n_\omega\rangle &= \langle n_\omega+1|-\sin\varphi\, Q_x\,\vec{e}_x+\cos\varphi\, Q_y\,\vec{e}_y|n_\omega\rangle\\ &= \langle n_\omega+1|Q_{\mathrm{E1}}|n_\omega\rangle(-\sin\varphi\;\vec{e}_x+\cos\varphi\;\vec{e}_y)\end{aligned} \tag{A1}$$

and

$$\langle n_\omega+1|Q_{\mathrm{E1}}|n_\omega\rangle^2=\left[\frac{\hbar(1+n_\omega)}{2V\omega_{\mathrm{TO,E1}}}\right]S_{\mathrm{p,E1}}(\omega). \tag{A2}$$

The phonon strength $S_{\mathrm{p,E1}}(\omega)$ in Eq. (A2) is

$$S_{\mathrm{p,E1}}(\omega)=\frac{\omega\omega_{\mathrm{TO,E1}}(\omega_{\mathrm{LO,E1}}^2-\omega_{\mathrm{TO,E1}}^2)}{(\omega_{\mathrm{TO,E1}}^2-\omega^2)^2+\omega_{\mathrm{TO,E1}}^2(\omega_{\mathrm{LO,E1}}^2-\omega_{\mathrm{TO,E1}}^2)}. \tag{A3}$$

This expression corresponds to the phonon strength of the threefold degenerate TO-phonon of crystals with zincblende structure which was derived by Mills and Burstein.[25]

2. Extraordinary mode $\vec{Q}_{\mathrm{Te}}$

We obtain

$$\begin{aligned}&\langle n_\omega+1|\vec{Q}_{\mathrm{Te}}|n_\omega\rangle\\ &\quad=\langle n_\omega+1|-\cos\varphi\,\cos\theta\;Q_x\,\vec{e}_x-\sin\varphi\,\cos\theta\,Q_y\,\vec{e}_y\\ &\qquad+\sin\theta\,Q_z\,\vec{e}_z|n_\omega\rangle\\ &\quad=\langle n_\omega+1|-\cos\varphi\;\;Q_x\,\vec{e}_x-\sin\varphi\;Q_y\,\vec{e}_y|n_\omega\rangle\cos\theta\\ &\qquad+\langle n_\omega+1|\;Q_z\;|n_\omega\rangle\sin\theta\,\vec{e}_z\\ &\quad=\langle n_\omega+1|Q_{\mathrm{E1}}|n_\omega\rangle(-\cos\varphi\,\vec{e}_x-\sin\varphi\,\vec{e}_y)\cos\theta\\ &\qquad+\langle n_\omega+1|\;Q_{\mathrm{A1}}\;|n_\omega\rangle\sin\theta\,\vec{e}_z\end{aligned} \tag{A4}$$

and

$$\begin{aligned}&\langle n_\omega+1|\vec{Q}_{\mathrm{Te}}|n_\omega\rangle^2\\ &\quad=\left[\frac{\hbar(1+n_\omega)}{2V}\right]\left(\frac{S_{\mathrm{p,E1}}(\omega)}{\omega_{\mathrm{TO,E1}}}\cos^2\theta+\frac{S_{\mathrm{p,A1}}(\omega)}{\omega_{\mathrm{TO,A1}}}\sin^2\theta\right).\end{aligned} \tag{A5}$$

The phonon strength $S_{\mathrm{p,E1}}(\omega)$ is given in Eq. (A3) and the phonon strength $S_{\mathrm{p,A1}}(\omega)$ is

$$S_{\mathrm{p,A1}}(\omega)=\frac{\omega\omega_{\mathrm{TO,A1}}\left(\omega_{\mathrm{LO,A1}}^2-\omega_{\mathrm{TO,A1}}^2\right)}{\left(\omega_{\mathrm{TO,A1}}^2-\omega^2\right)^2+\omega_{\mathrm{TO,A1}}^2\left(\omega_{\mathrm{LO,A1}}^2-\omega_{\mathrm{TO,A1}}^2\right)}. \tag{A6}$$

In the derivation in Ref. 24 exponents are erroneously placed in Eq. (30). $\omega_{T\perp}^2(\omega_{T\|}^2)$ should be replaced by $\omega_{T\perp}(\omega_{T\|})$ and in Eq. (31)[24] the expressions $(\omega_{T\perp}^2-\omega^2)((\omega_{T\|}^2-\omega^2))$ by $(\omega_{T\perp}^2-\omega^2)^2((\omega_{T\|}^2-\omega^2)^2)$.

For $\theta=0°$ we have polaritons of pure E_1 symmetry and for $\theta=90°$ of pure A_1 symmetry. For $\theta=0°$ the extraordinary transverse mode is degenerate with the ordinary polariton mode.

3. Extraordinary mode $\vec{Q}_{\mathrm{Le}}$

In close analogy to the results in the last subsection we obtain

$$\begin{aligned}&\langle n_\omega+1|\vec{Q}_{\mathrm{Le}}|n_\omega\rangle^2\\ &\quad=\left[\frac{\hbar(1+n_\omega)}{2V}\right]\left(\frac{S_{\mathrm{p,E1}}(\omega)}{\omega_{\mathrm{TO,E1}}}\sin^2\theta+\frac{S_{\mathrm{p,A1}}(\omega)}{\omega_{\mathrm{TO,A1}}}\cos^2\theta\right).\end{aligned} \tag{A7}$$

For $\theta=90°$ we have longitudinal modes of pure E_1 symmetry and for $\theta=0°$ longitudinal modes of pure A_1 symmetry.

In the limiting cases of phonons with symmetry E_1 and A_1 we obtain $S_{\mathrm{p,E1}}(\omega_{\mathrm{TO,E1}})=1$, $S_{\mathrm{p,A1}}(\omega_{\mathrm{TO,A1}})=1$ and $S_{\mathrm{p,E1}}(\omega_{\mathrm{LO,E1}})=\omega_{\mathrm{TO,E1}}/\omega_{\mathrm{LO,E1}}$, $S_{\mathrm{p,A1}}(\omega_{\mathrm{LO,A1}})=\omega_{\mathrm{TO,A1}}/\omega_{\mathrm{LO,A1}}$.

[1]H. Morkoc, S. Strite, G. Gao, M. Lin, B. Sverdlov, and M. Burns, J. Appl. Phys. **76**, 1363 (1994).
[2]S. Nakamura, T. Mukai, and M. Senoh, Appl. Phys. Lett. **64**, 1687 (1994).
[3]S. Nakamura, Solid State Commun. **102**, 237 (1997).
[4]I. Akasaki and H. Amano, Jpn. J. Appl. Phys., Part 1 **36**, 5393 (1997).
[5]J. S. Speck and S. F. Chichibu, MRS Bull. **34**, 304 (2009).
[6]C. Röder, F. Lipski, F. Habel, G. Leibiger, M. Abendroth, C. Himcinschi, and J. Kortus, J. Phys. D: Appl. Phys. **46**, 285302 (2013).
[7]M. Barchuk, C. Röder, Y. Shashev, G. Lukin, M. Motylenko, J. Kortus, O. Pätzold, and D. Rafaja, J. Cryst. Growth **386**, 1 (2014).
[8]Y. Huang, X. D. Chen, S. Fung, C. D. Beling, C. C. Ling, Z. F. Wei, S. J. Xu, and C. Y. Zhi, J. Appl. Phys. **96**, 1120 (2004).
[9]Y. Huang, X. D. Chen, S. Fung, C. D. Beling, and C. C. Ling, J. Phys. D: Appl. Phys. **37**, 2814 (2004).
[10]B. Ma, D. Jinno, H. Miyake, K. Hiramatsu, and H. Harima, Appl. Phys. Lett. **100**, 011909 (2012).
[11]K. Ishioka, K. Kato, N. Ohashi, H. Haneda, M. Kitajima, and H. Petek, J. Phys.: Condens. Matter **25**, 205404 (2013).
[12]M. V. Klein, "Electronic Raman scattering," in *Light Scattering in Solids I* (Springer-Verlag, 1983), p. 147.
[13]G. Abstreiter, M. Cardona, and A. Pinczuk, "Light scattering by free carrier excitations in semiconductors," in *Light Scattering in Solids IV* (Springer-Verlag, 1984), p. 5.
[14]G. Irmer, V. V. Toporov, B. H. Bairamov, and J. Monecke, Phys. Status Solidi B **119**, 595 (1983).
[15]W. L. Faust and C. H. Henry, Phys. Rev. Lett. **17**, 1265 (1966).
[16]M. Cardona, "Resonance phenomena," in *Light Scattering in Solids II* (Springer-Verlag, 1982) p. 19.
[17]T. Kozawa, T. Kachi, H. Kano, Y. Taga, M. Hashimoto, N. Koide, and K. Manabe, J. Appl. Phys. **75**, 1098 (1994).
[18]C. Wetzel, W. Walukiewicz, and J. W. Ager III, in *Symposium N-III-V-Nitrides*, edited by F. A. Ponce, T. D. Moustakas, I. Akasaki, and B. A. Monemar (Mater. Res. Soc. Symp. Proc., 1997), Vol. 449, p. 567.
[19]F. Demangeot, J. Frandon, M. A. Renucci, N. Grandjean, B. Beaumont, J. Massies, and P. Gibart, Solid State Commun. **106**, 491 (1998).
[20]H. Harima, H. Sakashita, and S. Nakashima, Mater. Sci. Forum **264–268**, 1363 (1998).
[21]H. Harima, H. Sakashita, T. Inoue, and S. Nakashima, J. Cryst. Growth **189/190**, 672 (1998).
[22]C. A. Arguello, D. L. Rousseau, and S. P. S. Porto, Phys. Rev. **181**, 1351 (1969).

[23]R. Claus, L. Merten, and J. Brandmüller, *Light Scattering by Phonon-Polaritons*, Springer Tracts in Modern Physics 75, edited by G. Höhler (Springer-Verlag, 1975).
[24]G. Irmer, C. Röder, C. Himcinschi, and J. Kortus, Phys. Rev. B **88**, 104303/1 (2013).
[25]D. L. Mills and E. Burstein, Rep. Prog. Phys. **37**, 817 (1974).
[26]In the original phrasing by Faust and Henry,[15] the Faust-Henry coefficient is derived for cubic crystals, based on the lattice equation of motion and often written in the form $C^{FH} = \frac{e^*}{\mu\omega_{TO}^2} \times \frac{(\partial\chi/\partial u)}{(\partial\chi/\partial E)}$ with the microscopic parameters dynamical charge e^* and reduced atom mass of the two sublattices μ, the derivations of the polarizability χ are with respect to the atomic displacement u and the electric field strength E. Our derivation for wurtzite crystals is based on the Born-Huang dynamical equations which describe phonons and phonon-polaritons as well. In these equations, all coefficients can be interpreted and measured macroscopically. For cubic crystals we obtain $C^{FH} = \frac{\sqrt{\varepsilon_0(\varepsilon_s-\varepsilon_\infty)}}{\omega_{TO}} \times \frac{(\partial\chi/\partial Q)}{(\partial\chi/\partial E)}$, written in SI units. The correspondence between the two formulae can be seen using $\omega_{LO}^2 - \omega_{TO}^2 = \frac{e^{*2}}{V_0\mu\varepsilon_0\varepsilon_\infty}$ (see, e.g., Eq. (2.86a) in Cardona[16]), the Lyddane-Sachs-Teller relation $\omega_{LO}^2/\omega_{TO}^2 = \varepsilon_s/\varepsilon_\infty$ and the definition $Q = \sqrt{\mu/V_0}u$ of the generalized displacement in the Born-Huang equations, V_0 is the volume of the unit cell.
[27]T. C. Damen, S. P. S. Porto, and B. Tell, Phys. Rev. **142**, 570 (1966).
[28]G. Yu, H. Ishikawa, T. Egawa, T. Soga, J. Watanabe, T. Jimbo, and M. Umeno, Jpn. J. Appl. Phys., Part 2 **36**, L1029 (1997).
[29]V. Y. Davydov, Y. E. Kitaev, I. N. Goncharuk, A. N. Smirnov, J. Graul, O. Semchinova, D. Uffmann, M. B. Smirnov, A. P. Mirgorodsky, and R. A. Evarestov, Phys. Rev. B **58**, 12899 (1998).
[30]The $E_{2,high}$ phonon is not allowed in polarization configurations with laser polarization and/or scattered light polarization parallel to the $z(c)$ axis of the crystal (see Table I). For normalization of all spectra recorded with one scattering setup and different polarization configurations we used the intensity of the $E_{2,high}$ phonon in spectra obtained in the (yy) or (xx) polarization. In order to check the reliability of this procedure and to exclude influences of the apparatus we measured the depolarized CCl_4 bands at 217 cm^{-1} and 315 cm^{-1} in four polarization combinations. The determined depolarization ratio was 0.75 ± 0.02 as expected.
[31]In estimations neglecting the influence of the plasmon damping the carrier concentration n is overestimated. The overestimation increases with decreasing carrier mobility. For large carrier mobilities ($\mu > 1000\,cm^2/V\,s$, exceptionally high) the error is small but in case of more realistic mobilities the carrier concentration is estimated too high up to a factor of two (for $\mu = 50\,cm^2/V\,s$ and n in the range of $10^{17}\,cm^{-3}$ to $5 \times 10^{18}\,cm^{-3}$).
[32]D. Kirillov, H. Lee, and J. S. Harris, Jr., J. Appl. Phys. **80**, 4058 (1996).
[33]F. Demangeot, J. Frandon, M. A. Renucci, C. Meny, O. Briot, and R. L. Aulombard, J. Appl. Phys. **82**, 1305 (1997).
[34]M. Klose, R. Dassow, M. Gross, and H. Schroeder, J. Cryst. Growth **189/190**, 666 (1998).
[35]M. Park, J. J. Cuomo, B. J. Rodriguez, W.-C. Yang, R. J. Nemanich, and O. Ambacher, J. Appl. Phys. **93**, 9542 (2003).
[36]H. Harima, T. Inoue, S. Nakashima, K. Furukawa, and M. Taneya, Appl. Phys. Lett. **73**, 2000 (1998).
[37]B. J. Skromme, K. C. Palle, C. D. Poweleit, H. Yamane, M. Aoki, and F. J. DiSalvo, Appl. Phys. Lett. **81**, 3765 (2002).
[38]H. Harima, J. Phys.: Condens. Matter **14**, R967 (2002).
[39]V. V. Emtsev, V. Y. Davydov, V. V. Kozlovskii, V. V. Lundin, D. S. Poloskin, A. N. Smirnov, N. M. Shmidt, A. S. Usikov, J. Aderhold, H. Klausing, D. Mistele, T. Rotter, J. Stemmer, O. Semchinova, and J. Graul, Semicond. Sci. Technol. **15**, 73 (2000).
[40]M. Kuball, Surf. Interface Anal. **31**, 987 (2001).
[41]I. Loa, S. Gronemeyer, C. Thomson, O. Ambacher, D. Schikora, and D. J. As, J. Raman Spectrosc. **29**, 291 (1998).
[42]G. Pezzotti, H. Sueoka, A. A. Porporati, M. Manghnani, and W. Zhu, J. Appl. Phys. **110**, 013527/1 (2011).
[43]P. Perlin, J. Camassel, W. Knap, T. Taliercio, J. C. Chervin, T. Suski, I. Grzegory, and S. Porowski, Appl. Phys. Lett. **67**, 2524 (1995).
[44]V. N. Bessolov, E. V. Konenkova, Y. V. Zhilyaev, and B. A. Paez Sierra, Appl. Surface Science **235**, 274 (2004).
[45]G. Popovici, G. Y. Xu, A. Botchkarev, W. Kim, H. Tang, A. Salvador, H. Morkoc, R. Strange, and J. O. White, J. Appl. Phys. **82**, 4020 (1997).
[46]R. Kirste, S. Mohn, M. R. Wagner, J. S. Reparaz, and A. Hoffmann, Appl. Phys. Lett. **101**, 041909/1 (2012).
[47]D. I. Florescu, V. M. Asnin, F. H. Pollak, R. J. Molnar, and C. E. C. Wood, J. Appl. Phys. **88**, 3295 (2000).
[48]C. Wetzel, W. Walukiewicz, E. E. Haller, J. Ager III, I. Grzegory, S. Porowski, and T. Suski, Phys. Rev. B **53**, 1322 (1996).
[49]K. Jeganathan, R. K. Debnath, R. Meijers, T. Stoica, R. Calarco, D. Gruetzmacher, and H. Lueth, J. Appl. Phys. **105**, 123707/1 (2009).